(*S*)-4-(3-^{18}F-Fluoropropyl)-L-Glutamic Acid: An ^{18}F-Labeled Tumor-Specific Probe for PET/CT Imaging—Dosimetry

Kamilla Smolarz[1], Bernd Joachim Krause[1], Frank-Philipp Graner[1], Franziska Martina Wagner[1], Christina Hultsch[2], Claudia Bacher-Stier[2], Richard B. Sparks[3], Susan Ramsay[3], Lüder M. Fels[2], Ludger M. Dinkelborg[2,4], and Markus Schwaiger[1]

[1]*Department of Nuclear Medicine, Klinikum rechts der Isar, Technische Universität München, München, Germany;* [2]*Bayer Healthcare, Berlin, Germany;* [3]*CDE Dosimetry Services Inc., Knoxville, Tennessee; and* [4]*Piramal Imaging GmbH, Berlin, Germany*

The glutamic acid derivative (*S*)-4-(3-^{18}F-Fluoropropyl)-L-glutamic acid (^{18}F-FSPG, alias BAY 94-9392), a new PET tracer for the detection of malignant diseases, displayed promising results in non–small cell lung cancer patients. The aim of this study was to provide dosimetry estimates for ^{18}F-FSPG based on human whole-body PET/CT measurements. **Methods:** ^{18}F-FSPG was prepared by a fully automated 2-step procedure and purified by a solid-phase extraction method. PET/CT scans were obtained for 5 healthy volunteers (mean age, 59 y; age range, 51–64 y; 2 men, 3 women). Human subjects were imaged for up to 240 min using a PET/CT scanner after intravenous injection of 299 ± 22.5 MBq of ^{18}F-FSPG. Image quantification, time–activity data modeling, estimation of normalized number of disintegrations, and production of dosimetry estimates were performed using the RADAR (RAdiation Dose Assessment Resource) method for internal dosimetry and in general concordance with the methodology and principles as presented in the MIRD 16 document. **Results:** Because of the renal excretion of the tracer, the absorbed dose was highest in the urinary bladder wall and kidneys, followed by the pancreas and uterus. The individual organ doses (mSv/MBq) were 0.40 ± 0.058 for the urinary bladder wall, 0.11 ± 0.011 for the kidneys, 0.077 ± 0.020 for the pancreas, and 0.030 ± 0.0034 for the uterus. The calculated effective dose was 0.032 ± 0.0034 mSv/MBq. Absorbed dose to the bladder and the effective dose can be reduced significantly by frequent bladder-voiding intervals. For a 0.75-h voiding interval, the bladder dose was reduced to 0.10 ± 0.012 mSv/MBq, and the effective dose was reduced to 0.015 ± 0.0010 mSv/MBq. **Conclusion:** On the basis of the distribution and biokinetic data, the determined radiation dose for ^{18}F-FSPG was calculated to be 9.5 ± 1.0 mSv at a patient dose of 300 MBq, which is of similar magnitude to that of ^{18}F-FDG (5.7 mSv). The effective dose can be reduced to 4.5 ± 0.30 mSv (at 300 MBq), with a bladder-voiding interval of 0.75 h.

Key Words: PET; radiation dosimetry; FSPG; oncology

J Nucl Med 2013; 54:861–866
DOI: 10.2967/jnumed.112.112581

The most frequently used tracer for PET imaging in cancer patients is ^{18}F-FDG. The increased glucose uptake into cells and the increased glycolysis, the so-called Warburg effect, are used in ^{18}F-FDG PET imaging (*1,2*). Glucose is not the only substrate with increased turnover in cancer cells. ^{18}F-labeled compounds tracing deranged metabolic pathways other than glycolysis may have advantages in situations in which ^{18}F-FDG has limitations. The amino acids glutamine and glutamate play important roles. Glutamine is the most abundant amino acid in the blood (*3*) and is used in tumors as a major anaplerotic substrate to produce energy and biomass by a truncated tricarboxylic acid cycle; blood levels of glutamate are usually much lower (*4*). Glutamine enters the cells via glutamine transporters and is rapidly converted by glutaminase to glutamate, leading to high intracellular concentrations of glutamate. Glutamate is either used as an anaplerotic substrate and consumed during glutaminolysis or used for glutathione biosynthesis or as an exchange substrate by the system x_C^- transporter (*5,6*). This exchanger binds glutamate and cystine with similar affinity and is able to transport both into the cells by exchange of abundant intracellular glutamate. Intracellularly, cystine is rapidly reduced to 2 molecules of cysteine, which are either used in glutathione biosynthesis or contribute directly to redox maintenance. A constant supply of glutathione and redox maintenance are especially important in tumor cells as protection against reactive oxygen species and for tumor survival during therapeutic interventions. (*S*)-4-(3-^{18}F-fluoropropyl)-L-glutamate (^{18}F-FSPG, alias BAY 94-9392) is a novel agent for PET imaging and is specifically transported into cells via system x_C^-. The specificity of uptake was demonstrated recently in cell competition assays and cells with transporter knockdown (*6*). An excellent tumor visualization was achieved in animal tumor models (*7*). Biodistribution analysis in rodents showed a rapid blood clearance via

Received Nov. 4, 2012; revision accepted Jan. 3, 2013.
For correspondence or reprints contact: Kamilla Smolarz, Nuklearmedizinische Klinik und Poliklinik, Technische Universität München, Klinikum rechts der Isar, Ismaninger Strasse 22, 81675 München, Germany.
E-mail: kamilla.smolarz@tum.de
Published online Apr. 8, 2013.

the kidneys and low background activity (including in the brain), providing high contrast for tumor imaging (*7*). ^{18}F-FSPG PET that examines system x_C^- activity in vivo may provide additional information on adaptations of tumors against oxidative stress and provide the potential for better understanding of tumor biology and chemoresistance mechanisms.

Pilot clinical studies using ^{18}F-FSPG showed promising results in non–small cell lung cancer and breast cancer (*8*). The present study describes the biodistribution of ^{18}F-FSPG and estimated the whole-body (WB) radiation dose resulting from ^{18}F-FSPG in healthy subjects. Safety and suitability for clinical application from a radiodosimetric perspective were assessed. Radiation dosimetry calculations were performed using the RADAR (RAdiation Dose Assessment Resource) method for internal dosimetry as implemented in the OLINDA/EXM software and in general concordance with the methodology and principles as presented in the MIRD 16 document (*9,10*).

MATERIALS AND METHODS

Subjects

The Ethics Committee of the Klinikum rechts der Isar, Technische Universität München, granted approval for this proof-of-mechanism PET/CT study, and the Federal Office for Radiation Protection and Federal Institute for Drugs and Medical Devices authorized the study. Five healthy volunteers (2 men, 3 women; age range, 51–64 y) were recruited, and written informed consent was obtained from each subject before the screening examination. Demographic data of the volunteers recruited are given in Table 1. Inclusion criteria were age between 50 and 65 y, ability to provide written informed consent, and adequate function of major organs. Exclusion criteria were pregnancy, lactation, and prior history of cancer. At screening, the volunteers did not have any clinically significant abnormality on physical or laboratory examinations (including physical examination, heart rate, blood pressure, electrocardiogram, hematology, serum biochemistry, coagulation, and urine analysis). The physical and laboratory examinations were repeatedly performed within 6 h, at 24 h and 7 d after injection of ^{18}F-FSPG, with added attention devoted to the occurrence of adverse events.

An intravenous catheter was placed in the antecubital vein of each arm, to allow tracer administration through one catheter and blood sampling with the other catheter. To avoid occlusion between sampling, saline was used for line flushing. All voided urine from the time of injection and up to 5 h after injection was collected, and the time of voiding was recorded for each volunteer. A well counter detector (Wallac) was used for the measurement of activity in the urine samples. In addition, a standard with a known amount of activity and of exactly the same volume as the urine samples was also measured, together with the samples, to convert the counting rate of the urine samples into activity. The total amount of excreted radioactivity was determined by multiplying the activity measurements with the urine volumes.

Radiosynthesis

^{18}F-FSPG was obtained via an automated 2-step radiosynthesis. In a first step, radiolabeling of the precursor (nosylate precursor Di-tert-butyl (*S*)-*N*-(tert-butoxycarbonyl)-4-(3-{[(4-nitrobenzene) sulfonyl]oxy}propyl)-L-glutamate) with ^{18}F-fluoride was performed. ^{18}F-fluoride was produced with an in-house 10-MeV cyclotron (Siemens). In a second step, acidic hydrolysis was used to remove the protective groups. Purification of the tracer was achieved via a Sep-Pak system (*11*).

Quality control of the tracer was conducted with regard to radionuclidic purity, radiochemical purity, chemical purity, appearance, and physicochemical properties. The radiochemical purity was at least 90%. The specific activity of ^{18}F-FSPG was greater than 190 GBq/μmol based on high-performance liquid chromatography measurements (calibration curve with nonradioactive reference compound).

PET Protocol

PET/CT was performed with a Biograph 64 TruePoint PET/CT scanner (Siemens Medical Solutions). It is a lutetium oxyorthosilicate 3-dimensional scanner and has an axial field of view of 216 mm, 39 image slices, a slice thickness of 4.2 mm, and a spatial resolution of 4.4 mm at the center of the field of view (*12*). Low-dose CT was used for attenuation correction of the PET emission scans. Volunteers were scanned supine with their arms down. After a planning CT scan, a low-dose (120 kV; 25 mAs; pitch, 1.2; CareDose 4D [Siemens]), no-contrast, WB CT scan was obtained. CT data were reconstructed in a 512×512 voxel matrix.

The mean injected ^{18}F-FSPG activity via an antecubital vein was 300 ± 22.9 MBq (mean ± SD), with a range from 275 to 330 MBq (Table1).

The first PET acquisition was started instantly after injection. After an initial total-body scan (12 bed positions, 1 min per bed position), 6 sequential WB scans from the top of the head to mid thigh were conducted, with an axial extent of 1,536 mm (7 bed positions, 1 min per bed position initially and 4 min per bed position in the last 2 scans). Subjects were permitted to leave the scanner after the fifth and sixth ^{18}F-FSPG scans. An ultra-low-dose CT scan (120 kV; 11 mAs; CareDose 4D) from the head to mid thigh was obtained before each of the 2 last PET acquisitions. A calibration source with a known activity and volume was placed

TABLE 1
Subject Details and Injected Radioactivity of ^{18}F-BAY 94-9392

Subject no.	Sex	Age (y)	Specific activity (GBq/μmol)	Injected dose (MBq)
1101	F	58	361	283
1102	F	64	269	316
1103	M	57	199	275
1104	F	63	282	330
1105	M	51	433	295
Mean ± SD		58.6 ± 5.2	309 ± 90	300 ± 22.9

TABLE 2
^{18}F-FSPG Imaging Protocol

Scan	Time (min)	Axial extent of scan	Scan duration
Low-dose CT	−2	Total body	
1	0	Total body	1 min per bed position
2	12	WB	1 min per bed position
3	19	WB	1 min per bed position
4	26	WB	1 min per bed position
5	33	WB	1 min per bed position
Ultra-low-dose CT	149	WB	
6	150	WB	4 min per bed position
Ultra-low-dose CT	239	WB	
7	240	WB	4 min per bed position

Ultra-low-dose CT was performed when subject was repositioned on scanner after getting up for bladder voiding.

next to the head and imaged with each volunteer. The imaging sequence is described in Table 2.

PET images from the Biograph 64 Truepoint PET/CT scanner were reconstructed using the attenuation-weighted ordered-subset expectation maximization algorithm implemented by the manufacturer, using 8 iterations and 4 subsets. Reconstruction included attenuation and scatter correction based on the CT data. ^{18}F activities were decay-corrected to the time of injection and normalized to the total administered activity.

Blood Sampling

Blood samples from 4 volunteers were drawn at approximately 5, 10, 15, 20, 30, 45, 60, 120, and up to 240 min after injection of ^{18}F-FSPG, and the exact time point of the collection of each blood sample was recorded. Blood sampling was technically not possible in 1 volunteer. The blood cells were separated from the plasma by centrifugation. A well counter detector (Wallac) was used for the measurement of activity in the whole-blood and plasma samples. In addition, a standard with a known amount of activity and of exactly the same volume as the blood and plasma samples was also measured, together with the samples, to convert the counting rate of the blood and plasma samples into activity. The stability of the tracer in plasma was assessed by thin-layer chromatography using a preparative layer (PLC) silica gel plate (Merck) and n-butanol/aqua/acetic acid/ethanol (12/5/3/1.5) as developing solvent.

PET Data Analysis

The attenuation-corrected transverse image data slice planes were resliced into coronal images for each subject and each time point using custom software (CDE Dosimetry Services, Inc.). Regions of interest for all organs showing uptake above general body uptake were constructed on the coronal slices to create volumes of interest representing activity-containing organs or tissues. Where reasonable, some coronal slices were combined before region-drawing to reduce the number of regions of interest required to complete this process. The regions of interest that were drawn included the stomach wall, heart contents, kidneys, liver, marrow, pancreas, salivary glands, spleen, thyroid, and urinary bladder.

Activity in each volume of interest was determined by summing concentration results directly from the PET images, along with voxel volumes. For images that stopped at the mid-thigh level, activity in the upper thigh was used to estimate the off-image activity. For quality-assurance purposes, activity in each volume of interest was also determined using the calibration source imaged with each patient and the head-to-feet total-body first-image total counts. Activities were also normalized where necessary to account for 100% of the injected activity, ensuring that the absorbed doses were not underestimates.

Absolute activity was converted to fractions of administered activity by dividing by the total activity administered. Organ and tissue data were fit in a least-squares sense using nonlinear regression with sums of exponentials. Between 1 and 4 exponential terms were used, as appropriate.

The normalized number of disintegrations in units of hours was established by integrating these empirically determined sums of exponentials from time zero to infinity, taking into account physical decay. The remainder of the body-normalized number of disintegrations was determined by fitting the remainder of the body time–activity obtained by subtracting all organ activities from WB activity. The urinary bladder–normalized number of disintegrations was established using the parameters determined by fitting the WB activity data with a urinary bladder model as implemented in the OLINDA/EXM software (*9*), with a 3.5-h bladder-voiding interval.

Absorbed dose estimates for all target organs and organ dose estimates were determined using the OLINDA/EXM software (*9*). The radiation transport phantom selected within OLINDA/EXM software was the hermaphroditic adult male phantom. The effective dose (ED) was determined using the methodology described in ICRP publication 60 (*13*).

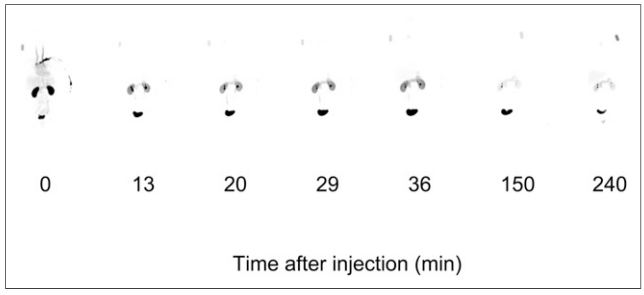

FIGURE 1. A 64-y-old healthy female volunteer. Maximum-intensity-projection PET images of 7 sequential WB images from 0 to 240 min after injection of 316 MBq of ^{18}F-FSPG.

RESULTS

All volunteers tolerated the examination well. All monitored parameters (electrocardiogram, blood pressure, and heart rate) stayed normal and unchanged during and after the examination. No study drug–related adverse event occurred. Laboratory blood tests were all normal and unchanged during and after the examination.

All volunteers showed fast clearance of the tracer from the blood pool, high uptake in the pancreas, and renal clearance resulting in high uptake in the kidneys and the bladder. Typical total-body PET biodistribution images of a subject from the first imaging time point at the time of intravenous injection of ^{18}F-FSPG up to 240 min after injection are shown in Figure 1. It is visually evident that there were high levels of accumulation of ^{18}F-FSPG in the kidneys, urinary bladder, and pancreas, whereas no significant levels of accumulation in the brain, lungs, breasts, liver, spleen, and intestines were identified.

Percentage injected activity as a function of time was determined for all quantified organs. On average, the organ that showed the largest peak uptake was the urinary bladder, with approximately 39% of the injected activity at 45 min after injection. The next largest peak uptake occurred in the kidneys at 10 min after injection, with approximately 16% of the injected activity. Figures 2A and 2B show time–activity curves (percentage injected dose per gram vs. time after injection) for selected organs for all subjects.

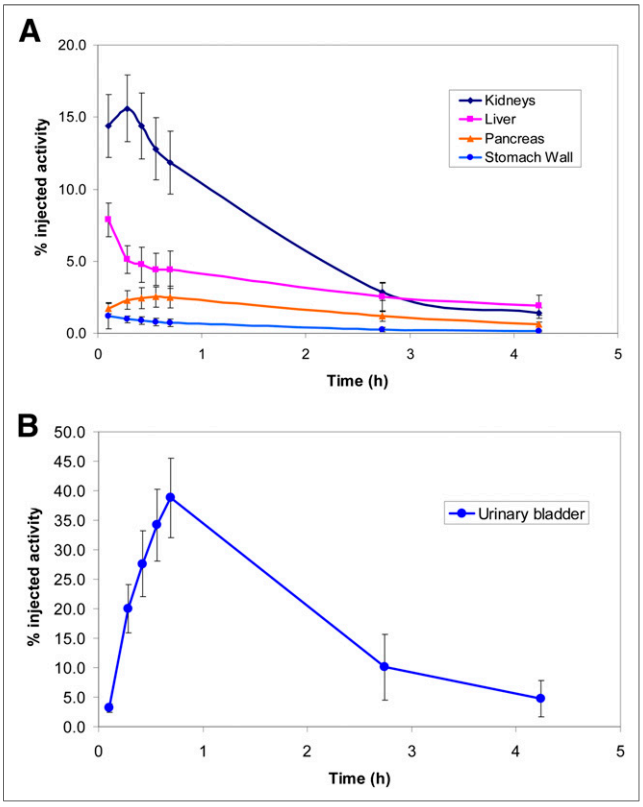

FIGURE 2. Mean time–activity curves for selected organs (kidneys, liver, pancreas, and stomach wall) (A) and urinary bladder (B) after injection of ^{18}F-FSPG in 5 healthy volunteers. Volunteers emptied their bladders after 0.75 and 3.0 h. Variability represented by error bars.

TABLE 3
Absorbed Dose Estimates (in mSv/MBq): Mean Values for 5 Subjects for Bladder-Voiding Time of 3.5 Hours

Organ	Mean
Adrenals	0.0094
Brain	0.0030
Breasts	0.0033
Gallbladder wall	0.0089
Lower large intestine wall	0.016
Small intestine	0.0097
Stomach wall	0.017
Upper large intestine wall	0.0087
Heart wall	0.011
Kidneys	0.11
Liver	0.014
Lungs	0.0045
Muscle	0.0069
Ovaries	0.015
Pancreas	0.077
Red marrow	0.0086
Osteogenic cells	0.0081
Salivary glands	0.0064
Skin	0.0040
Spleen	0.015
Testes	0.011
Thymus	0.0043
Thyroid	0.013
Urinary bladder wall	0.40
Uterus	0.030
Total body	0.0076
ED	0.032

The largest mean normalized number of disintegrations for the subjects was determined for the urinary bladder (0.85 h), remainder tissues (0.66 h), and kidneys (0.17 h). Table 3 lists organ-absorbed doses per unit administered activity (in mSv/MBq) as calculated using OLINDA/EXM software. On average, the organ receiving the largest absorbed dose was the urinary bladder at 0.40 ± 0.058 mSv/MBq, followed by the kidneys at 0.11 ± 0.011 mSv/MBq. On the basis of the organ-absorbed doses, the mean ED was estimated to be 0.032 ± 0.0034 mSv/MBq, with a low of 0.029 mSv/MBq and a high of 0.037 mSv/MBq. The ED resulting from a typical diagnostic activity of 300 MBq of ^{18}F-FSPG was estimated to be 9.5 ± 1.0 mSv. The highest organ dose to an individual subject observed in the study was 0.50 mSv/MBq to the urinary bladder, observed in a male subject.

Absorbed dose to the bladder and the ED can be reduced significantly by frequent bladder-voiding intervals. For a 0.75-h voiding interval, the urinary bladder dose was reduced to 0.10 ± 0.012 mSv/MBq and the ED to 0.015 ± 0.0010 mSv/MBq, or 4.5 ± 0.30 mSv at a 300-MBq dosing level.

^{18}F-FSPG was rapidly cleared from the blood pool, and within 30 min the percentage injected dose per gram value was less than 0.04, as shown in Figures 3A and 3B. Plasma values were higher than those of whole blood at all times.

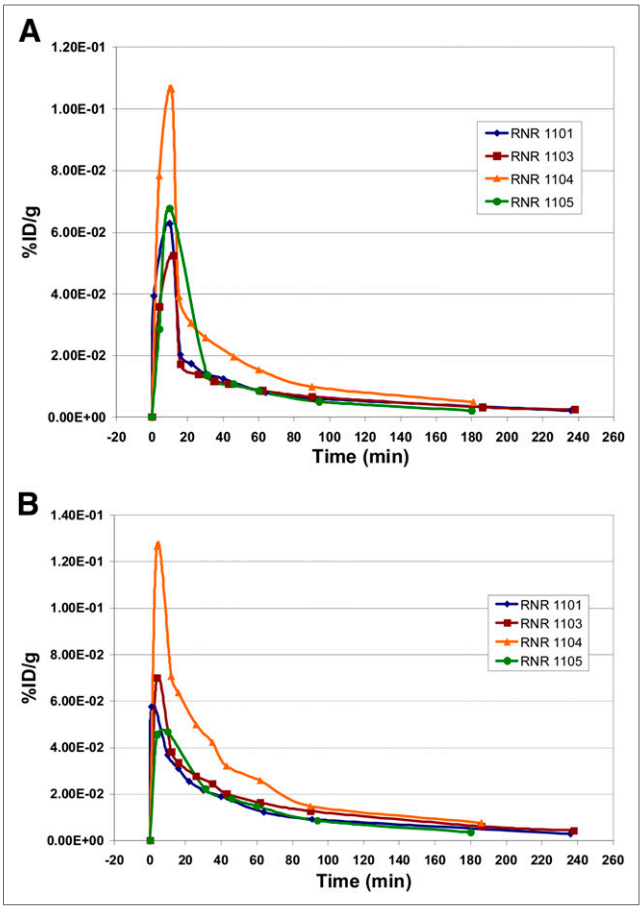

FIGURE 3. Time–activity curve in whole-blood samples (A) and in plasma samples (B). Measured data in 4 subjects; blood sampling for metabolite analysis was not performed in 1 subject.

No radiolabeled metabolites were detected in the plasma within 240 min after intravenous injection, with thin-layer chromatography detecting only the nonmetabolized ^{18}F-FSPG (Fig. 4).

DISCUSSION

The clinical safety and the WB biodistribution of ^{18}F-FSPG after the intravenous bolus administration were evaluated in healthy adult volunteers, and the associated internal radiation dosimetry was determined. In this study, the tracer was found to be safe and well tolerated, with no drug-related adverse event occurring in 5 subjects. The tracer showed predominant clearance through the kidneys and excretion of radioactivity into the urinary bladder. An increased initial activity concentration and slightly delayed clearance were observed for subject RNR1104; these might be mainly attributed to a suboptimal hydration status (Fig. 3). The renal clearance of ^{18}F-FSPG led to the urinary bladder receiving the highest absorbed doses. Uptake by the pancreas was relatively high.

^{18}F-FSPG was stable in humans; it did not show any defluorination or any other metabolites. Thin-layer chromatography documented only the intact tracer up to 240 min after injection. In our previous imaging study with ^{18}F-4-fluoro-L-glutamate (BAY 85-8050), we found characteristics similar to ^{18}F-FSPG, with fast clearance from the peripheral blood and renal excretion (*14*). However, BAY 85-8050 was not stable in humans and as early as 5 min after injection radiolabeled metabolites were detectable in plasma (*14*). We interpreted the reason for the instability as a systemic metabolism in human subjects, with subsequent uptake of fluorinated metabolites in the bone. ^{18}F-FSPG, by contrast, was stable in humans; no fluorinated metabolites were present in plasma during the examination up to 240 min after intravenous injection. The rapid clearance from the blood pool resulted in a low background in the brain, thorax, and intestines, allowing for potential tumor imaging in these regions.

On the basis of the biodistribution study in 5 healthy human subjects, we estimated the ED of ^{18}F-FSPG to be 9.5 mSv (with the potential to be lowered to 4.5 mSv with frequent bladder voids), which was comparable to other radiolabeled pharmaceuticals and the ED of ^{18}F-FDG. Table 4 summarizes the EDs of other ^{18}F-labeled radiopharmaceuticals (*15–18*) and ^{18}F-FSPG. In comparison to BAY 85-8050, the ED of ^{18}F-FSPG was calculated to be higher (*14*). ^{18}F-FSPG was solely excreted renally; the organ dose to the urinary bladder, in comparison to BAY 85-8050, was larger (0.40 mSv/MBq vs. 0.03 mSv/MBq) and was one of the factors that caused a larger ED.

^{18}F-FSPG visualizes a metabolic pathway, which is different from glycolysis, providing more insight into tumor biology and the metabolic requirements of tumors (*4,5*). Furthermore, ^{18}F-FSPG PET imaging studies could contribute to the further elucidation of the role of system x_C^- in oxidative stress and chemoresistance of tumors.

Because proliferating cells show an increased demand for amino acids, L-glutamine, the most abundant amino acid in the blood pool, may serve as adequate supply. The glutamine catabolism in the cancer cell is upregulated to function as a source of metabolic energy and as a precursor for

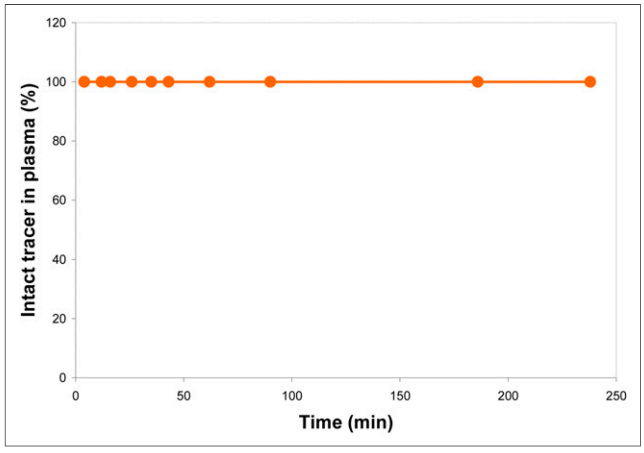

FIGURE 4. Thin-layer chromatography results in plasma (n = 4). Only intact tracer was detected.

TABLE 4
Comparison of ED Estimates for Several ^{18}F-Labeled Pharmaceuticals

Tracer	ED (mSv/MBq)
^{18}F-FSPG	0.032 ± 0.0034
^{18}F-FDG (*15*)	0.019
3′-deoxy-3′-^{18}F-fluorothymidine (*16*)	0.028 ± 0.012
O-(2-^{18}F-fluoroethyl)-L-tyrosine (*17*)	0.016
^{18}F-fluoromethylcholine (*18*)	0.031 ± 0.007

nonessential amino acid biosynthesis serving as a primary nitrogen donor (*19*). The increased glutaminolysis provides an anaplerotic substrate to replenish the intermediates in the truncated citric acid cycle and acts as an important energy source for the cell (*4*). The MYC oncogene, frequently dysregulated in human cancer, encodes a transcription factor, which stimulates the conversion of glutamine to glutamate (*20*). Imaging of the glutaminolytic and associated pathways may further elucidate the complex metabolic pathways involved in the tumor proliferation.

Preclinical studies demonstrated a high uptake of ^{18}F-FSPG in several tumor cell lines occurring specifically via the system x_C^-, a sodium-independent transporter, which has an increased activity in tumors (*7*). Proof-of-mechanism studies are currently under way describing promising results in humans, which will be important for the further development of ^{18}F-FSPG as an imaging agent in cancer.

CONCLUSION

This study was performed to describe the biodistribution and assess the radiation dose of ^{18}F-FSPG. The PET tracer ^{18}F-FSPG is safe. The dosimetry estimates presented in this study reveal a possible use of ^{18}F-FSPG from the dosimetric point of view. The radiation dose of ^{18}F-FSPG is of a magnitude similar to the ED of ^{18}F-FDG, the most commonly used tracer in oncology.

DISCLOSURE

The costs of publication of this article were defrayed in part by the payment of page charges. Therefore, and solely to indicate this fact, this article is hereby marked "advertisement" in accordance with 18 USC section 1734. The study was sponsored by Bayer HealthCare. No other potential conflict of interest relevant to this article was reported.

ACKNOWLEDGMENTS

We thank Yvonne Fischer, Sylvia Schachoff, and Anna Winter for their assistance with this study.

REFERENCES

1. Warburg O, Posener K, Negelein E. The metabolism of cancer cells. *Biochem Z.* 1924;152:309–344.
2. Mankoff DA, Eary JF, Link JM, et al. Tomography imaging in patients: fluorodeoxyglucose and beyond. *Clin Cancer Res.* 2007;13:3460–3469.
3. Bergström J, Furst P, Noree LO, et al. Intracellular free amino acid concentration in human muscle tissue. *J Appl Physiol.* 1974;36:693–697.
4. Russell R, Taegtmeyer H. Anaplerosis. In: Lennarz W and Lane MD, eds. *Encyclopedia of Biological Chemistry.* New York, NY: Academic Press. In press.
5. Bannai S, Kitamura E. Transport interaction of L-cystine and L-glutamate in human diploid fibroblasts in culture. *J Biol Chem.* 1980;255:2372–2376.
6. DeBerardinis RJ, Mancuso A, Daikhin E, et al. Beyond aerobic glycolysis: transformed cells can engage in glutamine metabolism that exceeds the requirement for protein and nucleotide synthesis. *Proc Natl Acad Sci USA.* 2007;104:19345–19350.
7. Koglin N, Mueller A, Berndt M, et al. Specific PET imaging of x_C- transporter activity using a ^{18}F-labeled glutamate derivative reveals a dominant pathway in tumor metabolism. *Clin Cancer Res.* 2011;17:6000–6011.
8. Baek S, Choi C-M, Ahn S, et al. Exploratory clinical trial of (4S)-4-(3-[^{18}F] fluoropropyl)-l-glutamate for Imaging x_c- transporter using positron emission tomography in patients with non–small cell lung or breast cancer. *Clin Cancer Res.* 2012;14:5427–.
9. Stabin MG, Sparks RB, Crowe E. OLINDA/EXM: the second generation personal computer software for internal dose assessment in nuclear medicine. *J Nucl Med.* 2005;46:1023–1027.
10. Siegel JA, Thomas SR, Stubbs JB, et al. MIRD pamphlet no. 16: techniques for quantitative radiopharmaceutical biodistribution data acquisition and analysis for use in human radiation dose estimates. *J Nucl Med.* 1999;40(suppl):37S–61S.
11. Berndt M, Schmitt-Willich H, Friebe M, et al., inventors. Method for production of F-18 labeled glutamic acid derivatives (Bayer Schering Pharma Aktiengesellschaft). Patent application WO 2011/060887. November 6, 2010.
12. Jakoby B, Long M, Carr C, Townsend D. Physical performance of a new combined PET/CT scanner [abstract]. *J Nucl Med.* 2007;48(suppl):46P.
13. International Commission on Radiological Protection (ICRP). *Recommendations of the International Commission on Radiological Protection*. Publication 60. Oxford, U.K.: Pergamon Press; 1991.
14. Krause B, Smolarz K, Graner F-P, et al. [^{18}F]BAY 85-8050 (TIM-1): a novel tumor specific probe for PET/CT imaging: dosimetry [abstract]. *J Nucl Med.* 2010;51(suppl 2):1434.
15. International Commission on Radiological Protection (ICRP). *Radiation Dose to Patients from Radiopharmaceuticals.* ICRP Publication 80: Addendum 2 to Publication 53. Oxford, U.K.: Pergamon Press; 1998.
16. Vesselle H, Grierson J, Peterson BA, Muzi M, Mankoff DA, Krohn KA. ^{18}F-Fluorothymidine radiation dosimetry in human PET imaging studies. *J Nucl Med.* 2003;44:1482–1488.
17. Pauleit D, Floeth F, Herzog H, et al. Whole-body distribution and dosimetry of *O*-(2-[^{18}F]fluoroethyl)-L-tyrosine. *Eur J Nucl Med Mol Imaging.* 2003;30:519–524.
18. DeGrado TR, Reiman RE, Timothy R, Price DT, Wang S, Coleman RE. Pharmacokinetics and radiation dosimetry of ^{18}F-fluorocholine. *J Nucl Med.* 2002;43:92–96.
19. Wise DR, DeBerardinis RJ, Mancuso A, et al. Myc regulates a transcriptional program that stimulates mitochondrial glutaminolysis and leads to glutamine addiction. *Proc Natl Acad Sci USA.* 2008;105:18782–18787.
20. Liu W, Le A, Hancock C, et al. Reprogramming of proline and glutamine metabolism contributes to the proliferative and metabolic responses regulated by oncogenic transcription factor c-MYC. *Proc Natl Acad Sci USA.* 2012;109:8983–8988.